

Brain mapping with Transcranial Magnetic Stimulation using a refined Correlation Ratio and Kendall's τ

L. Matthäus^{1*}, P. Trillenberg², T. Fadini³, M. Finke¹, and A. Schweikard¹

¹ Institute for Robotics and Cognitive Systems, University of Lübeck, Ratzeburger Allee 160, 23538 Lübeck, Germany, {matthaeus|schweikard}@rob.uni-luebeck.de

² Department of Neurology, University of Lübeck, Ratzeburger Allee 160, 23538 Lübeck, Germany, peter.trillenberg@neuro.uni-luebeck.de

³ Max-Planck-Institute for biophysical chemistry and Department of Clinical Neurophysiology, University of Göttingen, Robert-Koch-Str. 40, 37075 Göttingen, Germany, t.fadini@med.uni-goettingen.de

SUMMARY

Transcranial Magnetic Stimulation provides a mean to stimulate the brain non-invasively and painlessly. The effect of the stimulation hereby depends on the stimulation coil used and on its placement. This paper presents a mapping algorithm based on the assumption of a monotonous functional relationship between the applied electric field strength at the representation point of a muscle and the evoked motor potential. We combine data from coil characteristics, coil placement, and stimulation outcome to calculate a likelihood map for the representation of stimulated muscles

*Correspondence to: L. Matthäus, Institute for Robotics and Cognitive Systems, University of Lübeck, Ratzeburger Allee 160, 23538 Lübeck, Germany, matthaeus@rob.uni-luebeck.de

Contract/grant sponsor: T.F. was supported by an EC fellowship for Neuroscience Early Stage Research Training; contract/grant number: NEUREST, MEST-CT-2004-504193

in the brain. Hereby, Correlation Ratio (CR) and Kendall's rank coefficient τ are used to find areas in the brain where there is most likely a functional or monotonous relationship between electric field strength applied to this area and the muscle response. First results show a good accordance of our method with mapping from functional Magnetic Resonance Imaging.

In our case, classical evaluation of CR with binning is impossible, because sample data sets are too small and data is continuous. We therefore introduce a refined CR formula based on a Parzen windowing of the X -data to solve the problem. In contrast to usual windowing approaches, which require numeric integration, it can be evaluated directly in $O(n^2)$ time. Hence, its advantage lies in fast evaluation while maintaining robust applicability to small sample sets. We suggest that the presented formula can generally be used in CR related problems where sample size is small and data range is continuous. Copyright © 2007 John Wiley & Sons, Ltd.

1. Introduction

Transcranial Magnetic Stimulation (TMS) is an established method to stimulate the brain non-invasively and painlessly [1]. By placing a coil at the patient's head and sending an intense current impulse through the coil, the cortex beneath the coil is stimulated. The exact response depends on the electromagnetic characteristics of the coil, which are governed mainly by its shape, and the placement of the coil with respect to the head.

For a prominent subclass of coils, namely figure-of-eight shaped coils, several methods exists to predict from a number of stimulations with known coil position and known muscle response the representation area of this muscle in the brain [2, 3, 4, 5, 6]. All methods have in common that they implicitly require the strongest stimulation to be directly under the centre of the coil. For figure-of-eight shaped coils this is indeed the case, but for also widely used circular coils this is far from true. Here, the maximum stimulation is not localised directly under the coil

centre, but rather has the form of a circle underneath the coil rim [7]. Some new coil designs like the H-coil [8] also have no unique focus point, so the established TMS brain mapping methods fail in these cases. Thielscher and Kammer presented an alternative method which included the calculation of the electric field of the figure-of-eight coil and which could in principle be extended to other coil geometries [9]. The disadvantage of their method is the time consuming protocol required and the restriction to one stimulation line.

This article presents a general brain mapping algorithm suitable for all stimulating coils and an arbitrary set of coil positions. In contrast to most of the methods cited above, it requires the knowledge of the electric field produced by the coil additionally to the knowledge of the stimulation sites and the stimulation responses. The coil characteristics can be obtained either by simulation or, as we show in Section 3.2, by direct measurement.

The main idea of our algorithm is to find areas in the brain where there is high functional dependence or a high correspondence (monotonicity) between the applied electric field from stimulation and the resulting response to the stimulus [7]. We determine the degree of functional dependence between the electric field strengths X and the responses Y using Correlation Ratio $\eta(Y|X)$ and the degree of correspondence using Kendall's rank coefficient $\tau(X, Y)$.

The difficulty arising in the application of Correlation Ration is the small number of samples for evaluating η and their continuous range. Normally, in TMS only 20 to 40 samples can be acquired because of time constrains. Furthermore, the sample data is distributed continuously. This requires a new approach to evaluate Correlation Ratio. To our best knowledge we present the first formula which can reliably cope with a very low number of samples of continuous range. The main idea is to use a non-parametric regression scheme to estimate the conditional

expectation $E(Y|X)$. It will be shown that the choice of the Nadaraya-Watson kernel estimator [10, 11] results in a simple algebraic formula for the estimation of η , which can be evaluated in $O(n^2)$, n being the number of samples.

Our approach enables the solution of the brain mapping problem described above in less than 3 minutes by calculating the Correlation Ratio or Kendall's τ for 310,000 sample sets with 51 data pairs each. First results show a good accordance of the mapping with alternative data from fMRI, see Section 3.4.

2. Correlation Ratio and Kendall's τ

2.1. Definition

2.1.1. Correlation Ratio η Correlation Ratio, historically denoted as η , can be used to measure the functional dependence of two random variables $X, Y : \Omega \rightarrow \mathbb{R}$. It was introduced by K. Pearson in 1905 [12]. Its main application lies in ordinal statistics, but it has also been applied recently as a measure in multimodal image registration [13]. The Correlation Ratio of Y given X is defined as

$$\eta(Y|X) := \frac{\text{Var}[E(Y|X)]}{\text{Var}[Y]}, \quad (1)$$

where $E(Y|X)$ denotes the conditional expectation of Y given X . It is easy to show that $E(Y|X)$ is the best functional approximation of Y in L^2 , the vector space of square integrable random variables [14]. Thus, Correlation Ratio relates the total variance of Y to the Variance of the part of Y which is explained by X . See [13] for a geometric derivation of $\eta(Y|X)$ in L^2 . If X and Y are independent, $\eta(Y|X) = 0$, if $Y = f(X)$ for a measurable function f , $\eta(Y|X) = 1$.

2.1.2. Kendall's rank coefficient τ Kendall's rank coefficient τ measures the degree of correspondence between two rankings. If $\{(x_1, y_1), \dots, (x_n, y_n)\}$ are n realisations of (X, Y) , we define

$$C_{ij} = \begin{cases} 1 & \text{if } (x_i - x_j) \cdot (y_i - y_j) > 0 \\ 0 & \text{else} \end{cases}, \quad D_{ij} = \begin{cases} 1 & \text{if } (x_i - x_j) \cdot (y_i - y_j) < 0 \\ 0 & \text{else} \end{cases}.$$

Hence, $C := \sum_{i < j} C_{ij}$ is the number of concordant pairs, $D := \sum_{i < j} D_{ij}$ is the number of discordant pairs and the rank coefficient

$$\tau(X, Y) := \frac{C - D}{\frac{1}{2}n(n - 1)} \tag{2}$$

is a normalised measure of monotony of the relation of X and Y . If the relation is monotonously increasing, $\tau = 1$, if the relation is monotonously decreasing, $\tau = -1$.

A particularity requiring special attention is the case of equal sample values $x_i = x_j$ or $y_i = y_j$, because they lead to neither concordant nor discordant pairs, but are counted in the denominator. We chose to handle this using Kendall's τ b - formula, i.e. we replaced $\frac{1}{2}n(n - 1)$ by $\sqrt{C + D + n_y}\sqrt{C + D + n_x}$ with n_y denoting the number of pairs with $i < j$, $x_i = x_j$, $y_i \neq y_j$ and n_x denoting the number of pairs with $i < j$, $x_i = x_j$, $y_i \neq y_j$. For the implementation we used the algorithm suggested by [15].

2.2. A discrete Correlation Ratio formula for small continuous sample sets

This section discusses how to estimate η from a small number of sample pairs $\{(x_1, y_1), \dots, (x_n, y_n)\}$ of the continuous random variable (X, Y) .

The standard sample formula for η is given by

$$\eta(Y|X) = \frac{\sum_{i=1}^n \left(\frac{1}{n_{x_i}} \sum_{j=1}^{n_{x_i}} y_{x_i,j} - \bar{y} \right)^2}{\sum_{i=1}^n (y_i - \bar{y})^2} \tag{3}$$

where \bar{y} denotes the mean of $\{y_1, \dots, y_n\}$ and n_{x_i} denotes the number of Y -samples $y_{x_i,j}$ with the same X -value x_i . The use of formula (3) in our context is problematic, because the necessary introduction of artificial ‘‘bins’’ for X and the small sample size make the evaluation highly unstable. It should be noted that if X has ordinal values, one can improve (3) by choosing an unbiased evaluation of the variance as Kelley showed in 1935 [16]. Nevertheless, the fundamental problem of having too few values in artificial bins remains.

We avoid the problems associated with the introduction of bins for X -values by expressing η as

$$\begin{aligned}\eta(Y|X) &= \frac{\sum_{i=1}^n (E(Y|X = x_i) - \bar{y})^2}{\sum_{i=1}^n (y_i - \bar{y})^2} \\ &= \frac{n \sum_{i=1}^n E(Y|X = x_i)^2 - (\sum_{i=1}^n y_i)^2}{n \sum_{i=1}^n y_i^2 - (\sum_{i=1}^n y_i)^2}\end{aligned}\quad (4)$$

and finding a suitable expression for $E(Y|X = x_i)$. As mentioned in Section 2.1, $E(Y|X)$ is the function that approximates Y best given X . Because we have no a priori knowledge about the connection of X and Y , we employ a non-parametric regression model to estimate $E(Y|X)$ [17, 18]. As we will see in Section 3, evaluation speed is a concern in our case, so we decided to use the relatively simple Nadaraya-Watson kernel estimation for $E(Y|X)$ [10, 11].

The main idea of the Nadaraya-Watson kernel estimator is to approximate the density p_{XY} by a sum of product kernels $g_i \cdot h_i$, centred at (x_i, y_i) :

$$p_{XY}(x, y) \approx \frac{1}{n} \sum_{i=1}^n g_i(x) h_i(y). \quad (5)$$

This results in the following simple expression for $E(Y|X = x_i)$:

$$\begin{aligned}E(Y|X = x_i) &= \int_{\mathbb{R}} y p_{XY}(x_i, y) dy \\ &= \frac{1}{n} \sum_{j=1}^n g_j(x_i) y_j,\end{aligned}\quad (6)$$

i.e. an average of the y_j weighted by the kernels $g_j(x_i)$.

Expression (6) can be evaluated fast by a computer as soon as windowing functions g_j are defined. In our implementations, we took them to be Gaussian density functions with mean x_j and standard deviation σ . We set σ to ten times the average distance of an X -sample to its next neighbour. Note that other windowing functions are also perfectly valid, but the setting presented here was found to perform well for our application. Especially the rather broad setting of σ was found to yield very stable results for the brain mapping task described in Section 3.3.

Formula (6) has several advantages compared to binning (Equation (3)) or Parzen Windowing schemes [19]: Firstly, it has no “bins”, i.e. it can be used for discrete as well as for continuous sample values. Secondly, the result depends smoothly on the sample values x_i, y_i , if a smooth windowing function is chosen. Thirdly, it can be evaluated fast and stable with any windowing function (kernel) without further numeric theory. Fourthly, it gives stable results, even if the number of samples is very low, see Section 3.

3. Brain Mapping

After the theoretical foundation has been laid, we are now ready to describe our approach to brain mapping using statistical measures. We describe briefly in Sections 3.1 and 3.2 how the experimental data is obtained before we explain in Section 3.3 how Correlation Ratio and Kendall’s τ are used to calculate a likelihood map for the representation of a muscle in the brain. Section 3.4 finally presents results of our approach.

Although the underlying biophysical processes leading to a macroscopic response to TMS are still not completely clarified, it seems to be established that the effects of the stimulation

on the central nervous system are related to the strength of the electric field delivered to the representation site by the pulse [7, 9, 20]. The aim in brain mapping is now to identify the region in the brain where a muscle is represented from a number of stimulations at different sites around the head, the obtained muscle responses, and the electromagnetic characteristics of the coil.

3.1. Experimental Setup

A first set of mapping procedures were performed on a 27 years old, right handed, healthy male. Data was obtained in two separate sessions, denoted Experiment 1 and Experiment 2, with differing stimulator setup and differing mapping procedures. Details are given in the consecutive sections.

A second set of mapping procedures were performed on a 48 years old, right handed female with a oligoastrocytoma WHO grade III in the right central region. Data was obtained in one session, denoted Experiment 3, for stimulating the left hemisphere with a MagStim figure-of-eight coil. Details are given in the consecutive sections.

Informed consent for all procedures was given by both probands.

3.1.1. TMS TMS was applied as single biphasic pulse with interstimulus intervals of more than 2 seconds. TMS was delivered to the left hemisphere with a Medtronic MagPro X100 stimulator (Medtronic Inc., Minneapolis, MN, USA) and the circular MFC75 coil (Experiment 1) and with a MagStim Rapid² stimulator (The MagStim Company, Whitland, Dyfed, UK) with the standard figure-of-eight coil (Experiments 2, 3). In all experiments the coils were placed tangentially to the scalp with the coil centre touching the head slightly. Most accurate positioning was ensured using a robot and MRI based navigation, see Section 3.1.2. In

Experiments 2 and 3, the figure-of-eight coil was oriented with an angle of 45° (with the handle of the coil pointing to the back of the subject, namely the coil tip was pointing the nose of the subject) with respect to the medial line of the head. The circular coil in Experiment 1 was placed such as to enable easy positioning with the robot; this is unproblematic since the rotational symmetric electric field of the coil does not change with coil orientation.

Motor responses were recorded using Ag/AgCl electrodes and a Toennies-Multiniler IV (Jaeger-Toennies, Würzburg, Germany) hardware (Experiment 1) / CED 1401 (Cambridge Electronic Design, Cambridge, UK) hardware (Experiments 2, 3). Recording electrodes were placed on the thenar (abductor pollicis brevis muscle, APB) and on the hypotenar (abductor digiti minimi muscle, ADM). The signal was band-pass filtered between 1.6 Hz and 1 kHz and sampled at 5 kHz rate. The amplitude of the MEP was calculated from negative to positive peak. The subject was lying on a couch (Experiment 1) / sitting on an armchair with his arms supported (Experiments 2, 3), in a relaxed state. Relaxation has been checked by mean of EMG recordings.

3.1.2. Coil Navigation For every mapping procedure to work it is important to determine the stimulation sites with respect to the head. We briefly describe our method here, a comprehensive overview is given in [21, 22].

Basis for the mapping procedure is a magnetic resonance imaging (MRI) of the subject's head. Applying image segmentation algorithms, the head outline (cranium) and the grey matter surface (brain surface) are obtained. The segmented cranium is registered to the continuously tracked subject's head using surface points obtained from an optical tracking device, e.g. a Polaris infrared stereo camera (NDI, Ontario, Canada). A number of different stimulation sites are planned using the virtual cranium. This plan is then implemented by a

robot, steering the coil to its correct position relative to the patient's head. The coil is kept in place during the stimulation by active motion compensation.

3.1.3. Motor Response Second ingredient for each TMS motor mapping algorithm is the strength of response of a muscle to TMS delivered at a certain position. We have used two different protocols.

In the first protocol (Experiments 1, 3), we fixed the strength of the stimulator output to 100%. For the mapping procedure we took the three stimuli averaged peak-to-peak measures of the muscle response (in mV) at the different stimulation sites as Y -values (see Section 3.3). Note that this enabled us to measure the APB and the ADM muscle responses at the same time using multi-channel MEP recording.

In the second protocol (Experiment 2), we recorded the stimulator output used to perform the stimulation was that needed to elicit a MEP of 1mV peak-to-peak amplitude in 5 out of 10 stimuli. The recordings were expressed in form of percentage of the maximum output delivered by the device. So the measure indicating the response strength, the Y -values in our algorithm below, are the required stimulator strengths. Clearly, this protocol requires the mapping of ADM and APB muscle in two independent stimulation series.

We should remark that Protocol 2 gives more accurate and reproducible Y -values [9], but suffers from the fact that for coil positions far from the "Hot-spot" no stimulations with responses of 1mV can be obtained due to the limited strength of the simulator. Furthermore, this procedure is much more time consuming, reducing the number of stimulation sites, and is thus hardly applicable if more than two muscles are to be mapped in one TMS session.

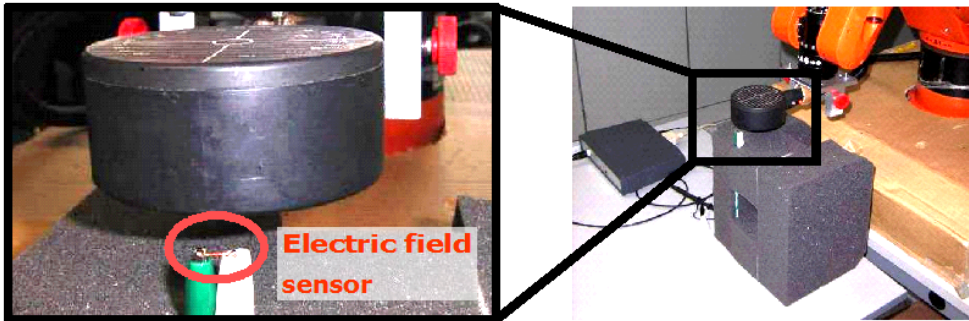


Figure 1. Measurement setup for obtaining the electric field produced by the MFC75 circular coil. The E-field is purely horizontal, thus inducing only a voltage in the horizontal wire probe.

3.2. Coil Data

Several different coil forms are in use for TMS. Most common are figure-of-eight coils, shaped like a double torus, and circular coils. Each coil stimulates the brain differently, because the electromagnetic field produced differs for each coil type. So to analyse the stimulation data, the characteristics of the coil must be known. Therefore we measured the electric field produced by the coil in a separate experiment.

In the absence of free charges and for low frequencies[†], the electric field \mathbf{E} produced by changing currents $I = I(t)$ in the coil with geometry c is given by [23, 24]

$$\mathbf{E}(r, t) = -\frac{\mu_0 \dot{I}(t)}{4\pi} \int_c \frac{d\hat{\mathbf{c}}}{|\mathbf{r} - \mathbf{c}|}. \quad (7)$$

Hereby, μ_0 denotes the permeability of free space, \dot{I} the change of the current flow in the coil, and $\hat{\mathbf{c}}$ the tangential vector along the coil curve c . As a direct consequence of (7), the electric

[†]A TMS pulse lasts about 100 μ s, yielding a frequency of 10 kHz. This is considered low, because the corresponding wavelength of $3 \cdot 10^4$ m is several orders of magnitude bigger than the head and the electric field sensor.

field of a planar coil, i.e. $\mathbf{c}_z \equiv 0$, has no vertical component. So by placing a small straight copper wire with geometry w horizontally beneath the coil and connect it via vertical running cables to an oscilloscope [25, 26], Fig. 1, the measured voltage at time t equals

$$V = \oint \mathbf{E} \cdot d\hat{\mathbf{S}} = \int_w \mathbf{E}(\mathbf{w}) \cdot d\hat{\mathbf{w}} \approx |w|\mathbf{E}(\mathbf{w}, t) \cos \phi, \quad (8)$$

where ϕ denotes the angle between wire direction and E-field direction. In (8) we assumed the wire length $|w|$ to be small, so that \mathbf{E} is constant along it.

By (7), the electric field of a circular coil is rotational symmetric and for $\mathbf{w}_y = 0$ holds $\mathbf{E}_x = 0$. So it is enough to measure the E-field in the $x - z$ -plane having the straight wire segment aligned with the y -axis, $\dot{\mathbf{w}}_x = \dot{\mathbf{w}}_z = 0$.

For the figure-of-eight coil, we measured \mathbf{E}_x and \mathbf{E}_y in two separate experiments with different probe orientation and combined the measures using Pythagoras' Theorem.

To obtain the full electromagnetic characteristics, we placed the coil at regularly spaced grid positions and invoked a stimulation pulse with 70% stimulator output. By measuring the induced voltage in the sensor (8) at each position, we obtained a grid of electric field strengths for the coil [27], Figure 2. The measurement series were completely automated, using a KUKA KR3 robot (KUKA GmbH, Augsburg, Germany) and a PCS100 8 bit digital oscilloscope (Velleman Components N.V., Gavere, Belgium) with a sampling frequency of 800kHz.

3.3. Mapping Algorithm

3.3.1. η and τ maps As mentioned above, we assume a monotonous functional dependence between the electric field strength E^r at the representation point \mathbf{p}^r of a muscle and the measured evoked muscle response Y , i.e. $Y = f(E^r)$. Note that f will not be linear and may have a discontinuity at the motor threshold. To measure the degree of functional dependence,

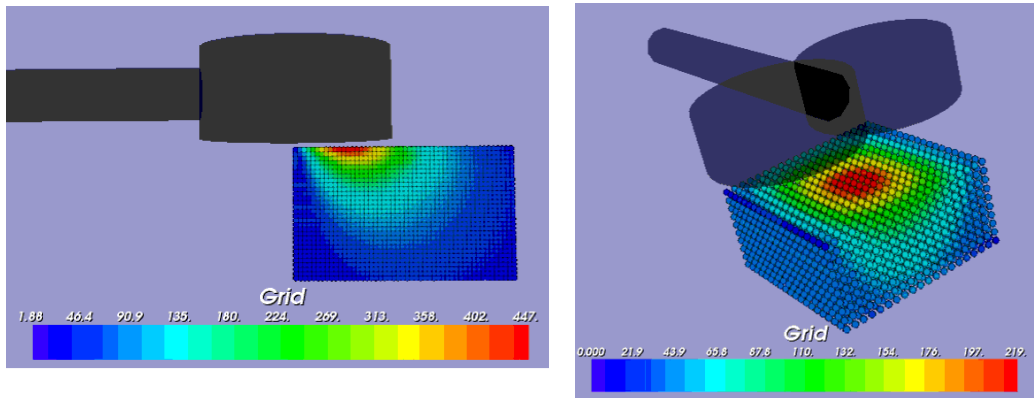


Figure 2. Electric field produced by the Medtronic MFC75 circular coil (left) and the MagStim figure-of-eight coil (right). The field of the circular coil is rotational symmetric, therefore only one radial slice is shown. The measures are given mV induced in the sensor. The grid comprises of 20×50 points, spaced at 2mm, for the circular coil, and $20 \times 20 \times 10$ points, spaced at 0.5mm, for the figure-of-eight coil. Note that for technical reasons the E-field map of the circular coil starts closer to the coil, hence the stronger maximum reading compared to the figure-of-eight coil.

Correlation Ratio is the statistic of choice to handle samples of E and Y and it holds

$$\eta(Y|E^r) = 1. \quad (9)$$

To measure the degree of correspondence between the electric field E^p at a point \mathbf{p} and the measured evoked muscle response Y , we use Kendall's τ and expect

$$\tau(E^r, Y) = 1. \quad (10)$$

Unfortunately, the true electric field strength at points in the brain is unknown, because the scalp, scull, cerebrospinal fluid, and brain weaken and distort the electric field produced by the coil. There have been many attempts to simulate those effects [9, 24]. But so far most models used only crude approximations of the true individual head and brain geometry (mainly using spherical head models). Furthermore, electromagnetic properties of the head tissues are not

well established and have been shown to possess great inter-individual differences [28]. As described in the next paragraphs, we require the knowledge of the electric field at all points at the brain surface for all stimulation points, creating a big computational task if modelling was used.

Instead we ignored the influence of the head on the electric field and used the measured electric field of the coils in air, from hereon denoted by X . So Equations (9), (10) become

$$\eta(Y|X^r) = 1 \quad (11)$$

$$\tau(X^r, Y) = 1. \quad (12)$$

If the distribution patterns of E and X do not differ too much, we expect our approach to be able to handle the inaccuracy induced by this approximation.

We consider each point \mathbf{p} on the brain surface separately. Firstly, we calculate the electric field strengths when firing the TMS coil at the stimulation sites $i = 1, \dots, n$. This is done with the help of the coil field map obtained as described in 3.2 and yields a list $\{x_1(\mathbf{p}), \dots, x_n(\mathbf{p})\}$. This list is different for each point \mathbf{p} , because even tiny changes in position \mathbf{p} lead to a different electric field strength at \mathbf{p} for fixed coil position, see Figure 2. Let $\{y_1, \dots, y_n\}$ be the list of measured motor responses as explained in Section 3.1.3. Note that this list is independent of \mathbf{p} .

Next, we calculate the Correlation Ratio value $\eta(y_1, \dots, y_n|x_1(\mathbf{p}), \dots, x_n(\mathbf{p}))$ and Kendall's τ value $\tau((x_1(\mathbf{p}), y_1), \dots, (x_n(\mathbf{p}), y_n))$ for \mathbf{p} . The values of η and τ change with \mathbf{p} because X changes with it. As explained above, if $\mathbf{p} = \mathbf{p}^r$, η and τ are expected to be 1. For all other points we expect them to be less than 1. For example, consider a remote point \mathbf{p}' , where the electric field strength of the coil is zero for all stimulation sites, $x_i(\mathbf{p}') = 0$, $i = 1, \dots, n$. This implies $E(Y|X(\mathbf{p}')) \equiv E(Y)$, hence $Var[E(Y|X(\mathbf{p}'))] = 0$ and $\eta(Y|X(\mathbf{p}')) = 0$. Similarly,

$C = D = 0$ in Equation (2), so $\tau(X(\mathbf{p}'), Y) = 0$.

For the final Correlation Ratio map we repeat the CR-calculation for every point on the brain surface. We evaluate $\eta(y_1, \dots, y_n | x_1(\mathbf{p}), \dots, x_n(\mathbf{p}))$ for each point \mathbf{p} separately and colour the point by its $\eta(\mathbf{p})$ value. Likewise, for the Kendall's τ map we repeat the τ -calculation for every point on the brain surface. We evaluate $\tau((x_1(\mathbf{p}), y_1), \dots, (x_n(\mathbf{p}), y_n))$ for each point \mathbf{p} separately and colour the point by its $\tau(\mathbf{p})$ value.

3.3.2. Centre of Gravity (CoG) As the projection of the centre of gravity of the measurements onto the cortex has been shown to give reasonable mapping results for figure-of-eight coils, [6], we compare our η and τ maps against this method for Experiments 2 and 3. Conventionally, the coil coordinates are weighted by the MEP response provoked when stimulated at this site and averaged. The resulting spot, which in general lies neither on the scalp nor on the cortex, is then projected to the cortex. Hereby, several projection methods exist, [5].

For Experiment 2 we adapted the Centre of Gravity method as follows: Let y_{max} be the maximum stimulator intensity for which we could evoke an MEP of 1mV. Define the centre of gravity point as

$$\mathbf{p}_{CoG}^{\text{variable stim output}} := \frac{\sum_{i=1}^{\tilde{n}} (y_{max} - y_i) \mathbf{p}_i}{\sum_{i=1}^{\tilde{n}} (y_{max} - y_i)}, \quad (13)$$

where y_i are the stimulator outputs in percent and \mathbf{p}_i are the stimulation sites. The sum runs only over the \tilde{n} stimulation sites for which we could evoke an MEP of 1mV.

For Experiment 3 we employed the standard formula

$$\mathbf{p}_{CoG}^{\text{variable MEP}} := \frac{\sum_{i=1}^n y_i \mathbf{p}_i}{\sum_{i=1}^n y_i}. \quad (14)$$

Our mapping value for a point \mathbf{p} on the cortex is then given as the normalised distance to \mathbf{p}_{CoG} . The normalisation is linear and such that the nearest cortex point has value 0, the

farthest has value 1. This gives similar results as the convex hull algorithm suggested by [5].

3.3.3. fMRI For comparison, functional magnetic resonance images (fMRI) of the brain were acquired for two finger movement tasks for Subject 1. Task one was to tip all fingertips of the right hand with the right thumb, yielding the brain activation area of the right APB. Task two consisted of spreading the right little finger sideways, activating mainly the area of the right ADM.

The paradigm used for each mapping was a block design with six volume data sets of activation and rest, respectively. Data were recorded on a 1.5T Siemens scanner with anatomical MRI resolution of 1mm and functional MRI resolution of 4mm. Data were analysed using SPM2 software [29] and visualised using MRIcro software [30].

Figure 3 displays the fMRI maps with thresholds of 12 for the APB task (range -8.4 – 17.9) and 6 for the ADM task (range -6.5 – 10.0). The coordinates[‡] of the maximum activation were (64, 106, 199) for the ADM muscle and (62, 111, 199) for the APB muscle, i.e. the APB-maximum is about 5mm anterior to the ADM-maximum.

3.4. Results

Three mapping experiments were performed as described in Section 3.1.3. In the experiments, η and τ values at 309,907 (Experiments 1, 2) and 252,333 (Experiment 3) points \mathbf{p} on the segmented brain surface were estimated using the algorithms presented in Section 2. The windowing functions g_i for η were taken to be Gaussians with standard deviation

[‡]All coordinate values in the paper are given in millimetres in MRI image coordinates; x -axis runs left to right, y -axis back to front, and z -axis upwards. The origin is in the bottom-left-back corner of the bounding box of the head.

$\sigma = 10 \frac{x_{max} - x_{min}}{n}$, i.e. ten times the average distance between two adjacent electric field strengths. Note that for every point \mathbf{p} the list of electric field strengths $x_i(\mathbf{p})$ differs and hence also σ changes. The calculation of η took about three minutes, the calculation of τ about one minute on a standard PC (mobile AMD Athlon 2500+ processor, 1.81 GHz, 768 MB RAM).

3.4.1. Experiment 1 MEP measurements at 34 coil positions were obtained for mapping with the circular coil. Coil positions were irregularly arranged roughly frontal to the central sulcus. Due to the lying position of the proband, more posterior positions could not be reached by the robot. The stimulation was given with a fixed intensity of 100% stimulator output at all positions, the reason for the unusual high choice of stimulator output being the invoice of muscle responses from as many stimulation sites as possible. The stimulation sites and resulting muscle responses are displayed in Figure 3 as colour-coded spheres.

To compensate for the lacking postcentral measurements, we added a ring of 17 artificial zero-measurements in big distance to the hot-spot to the data. Hence, Correlation Ratio and Kendall's τ were evaluated for 51 data pairs $(x_i(\mathbf{p}), y_i)$ for each point \mathbf{p} on the brain surface. Resulting Correlation Ratio values ranged from 0 to 0.72 for the ADM muscle and from 0 to 0.65 for the APB muscle. Resulting rank coefficient values τ ranged from 0 to 0.71 for the ADM muscle and for the APB muscle. The resulting maps are displayed in Figure 3. There, we set the maximum colour value to the maximum mapping value and the minimum colour value 15% below the maximum mapping value.

The maps for both muscles and both algorithms show a single, spatially sharply bounded maximum each. The coordinates for the maximum mapping value are given in Table I. The

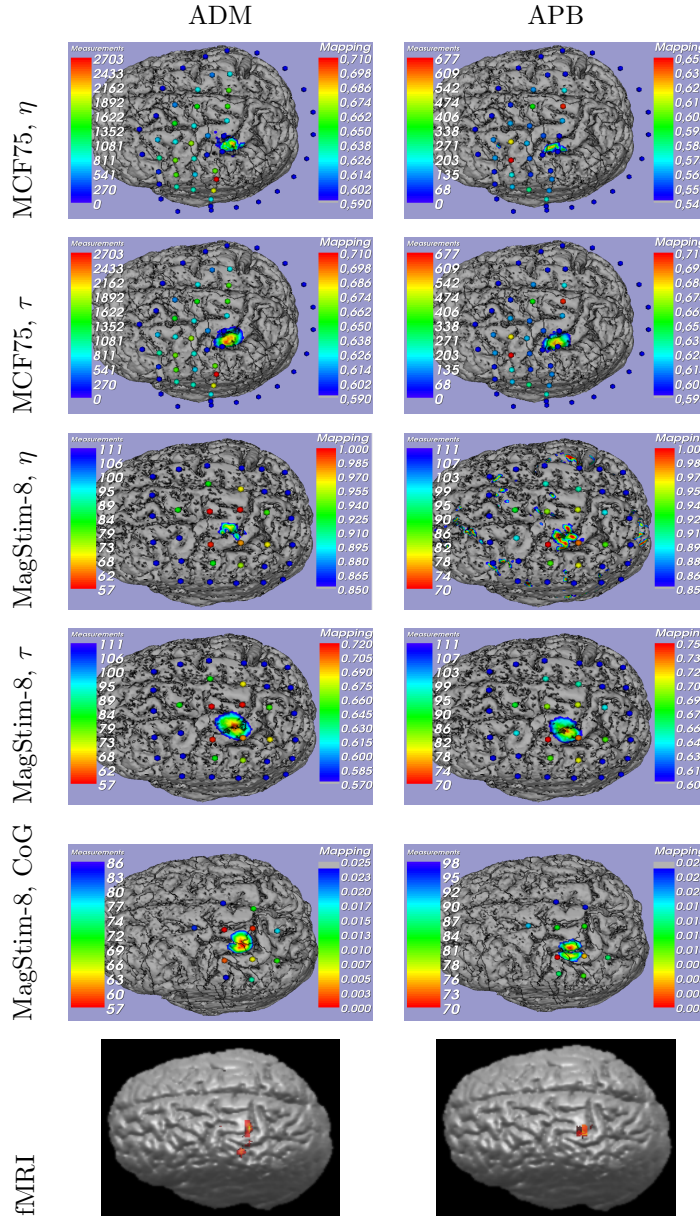


Figure 3. Results of the mapping calculations for ADM muscle (left) and APB muscle (right) for Experiments 1 and 2. The first two rows show experiment results for the Medtronic MCF75 circular coil, the third, fourth, and fifth row show experiment results for the MagStim figure-of-eight coil. The last row shows fMRI mapping for comparison. The spheres in the TMS pictures indicate the stimulation positions. The colour of the spheres encodes the obtained MEP signal (circular coil) and the stimulator output needed to obtain a muscle response of 1mV (figure-of-eight coil), respectively. Copyright © 2007 John Wiley & Sons, Ltd. *Statist. Med.* 2007; 00:0–0
Prepared using simauth.cls

The colour of a brain region depicts the Correlation Ratio value $\eta(Y|X(\mathbf{p}))$ (rows 1 and 3), Kendall's τ b - value $\tau(X(\mathbf{p}), Y)$ (rows 2 and 4), and the normalised distance from the centre of gravity (row 5). η and τ values give the likelihood that the mapped muscle is represented there. Mapping colours range from grey and blue (unlikely) to red (very likely).

	η	τ	fMRI
ADM	(54, 106, 196)	(54, 112, 197)	(64, 106, 199)
APB	(55, 118, 196)	(54, 113, 196)	(62, 111, 199)

Table I. Coordinates of the maxima for mapping the ADM and APB muscle using the Medtronic MCF75 circular coil. For comparison, fMRI maxima are given in the last column.

distances from the fMRI hot-spots[§] are 10 mm (ADM, η), 12 mm (ADM, τ), 10 mm (APB, η), 9 mm (APB, τ). All TMS mapping maxima are located lateral and anterior to the corresponding fMRI hot-spots. The distance between the η and τ mapping algorithm is 6 mm for the ADM and 5 mm for the APB. For the η algorithm the APB-maximum is about 5 mm anterior to the ADM-maximum. The ADM and APB maxima for the τ algorithm do nearly agree, but the area of high τ values for the APB is more anterior than for the ADM (Figure 3, second row). Anatomically, all areas of high TMS mapping value are located on the on posterior gyrus.

Figure 4 shows exemplarily the $(X(\mathbf{p}), Y)$ pairs for three different brain surface points \mathbf{p} and the ADM muscle. The points are chosen such that \mathbf{p}_0 is close to the η and τ maximum, \mathbf{p}_1 is close to the fMRI hot-spot (having intermediate η and τ value), and \mathbf{p}_2 has low η and τ value.

3.4.2. Experiment 2 As explained in Section 3.1.3, the maps obtained with the MagStim figure-of-eight coil according to Protocol 2 differed from the previously described maps. We did not record the muscle response, but the TMS-stimulator output to obtain a muscle response of 1mV peak-to-peak. This measure can be thought of inverse to the MEP measure, because

[§]Recall that the fMRI data spacing was 4mm, see Section 3.3.3

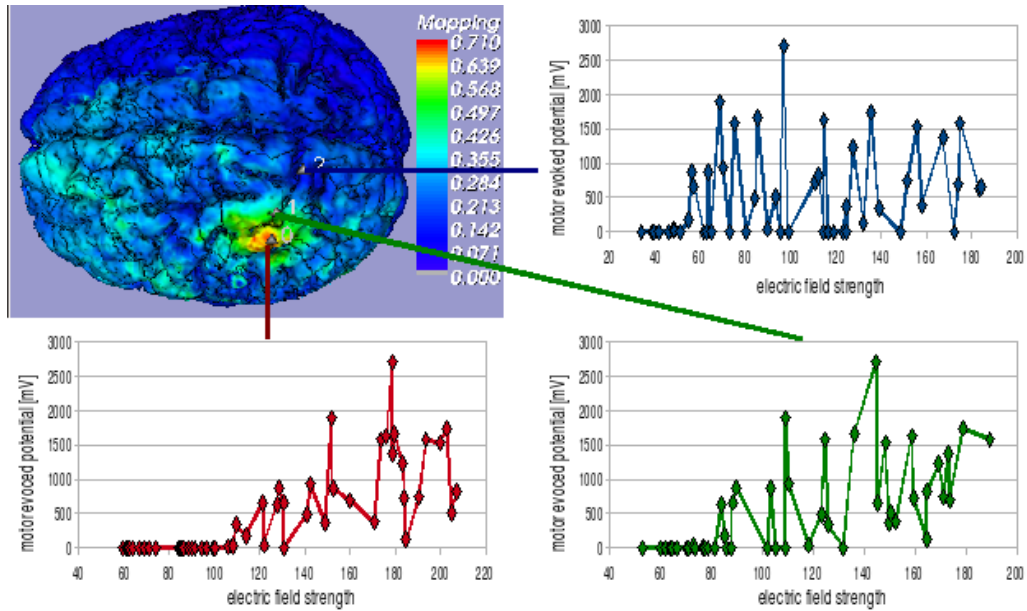


Figure 4. Experiment 1: Calculated electric field strength $X(\mathbf{p})$ (arbitrary units) and elicited MEP responses Y (peak to peak, in μV) at the ADM muscle for three different points on the brain surface. The points are chosen such that \mathbf{p}_0 is the Correlation Ration maximum point, \mathbf{p}_1 the fMRI hot-spot, and \mathbf{p}_2 a point with low η and τ value. Note that the Y -values are the same in all three graphs, only the respective X -values differ. The Correlation Ratio value at the points is $\eta_0 = 0.70$, $\eta_1 = 0.41$, and $\eta_2 = 0.14$; Kendall's rank coefficient value is $\tau_0 = 0.68$, $\tau_1 = 0.55$, $\tau_2 = 0.22$. The brain colour in the upper left picture is according to the Correlation Ratio value.

the stronger the muscle response to a fixed intensity stimulus the less intensity is needed to obtain a fixed muscle response. Nevertheless, we still assume

$$\eta(Y|X^r) = \eta(Y|X(\mathbf{p}^r)) = 1$$

to hold for the representation point \mathbf{p}^r , Y now being the stimulator output to elicit the 1mV motor response. For the rank coefficient τ we expect now negative values, because of the monotonously decreasing relationship between coil normalised field strength $X(\mathbf{p}^r)$ and the

	η	τ	CoG	fMRI
ADM	(65, 112, 200)	(63, 110, 197)	(62, 110, 200)	(64, 106, 199)
APB	(63, 110, 199)	(61, 112, 196)	(59, 113, 200)	(62, 111, 199)

Table II. Coordinates of the maxima (η, τ) / minima (CoG) for mapping the ADM and APB muscle using the MagStim figure-of-eight coil. For the (APB, η) mapping the maximum closest to the fMRI hot-spot was chosen. For comparison, fMRI maxima are given in the last column.

necessary stimulator output Y to elicit a muscle response of 1mV. To unify this scenario with the procedure from Experiment 1, we take $|\tau|$ as the mapping function and expect

$$|\tau(X^r, Y)| = |\tau(X(\mathbf{p}^r), Y)| = |-1| = 1.$$

In the experiment, 12 coil positions were used for mapping. Because calculating η out of 12 samples is very unstable, even with the algorithm presented above, we added 19 artificial measurement points far away from the hot-spot region. As discussed in Section 3.1.3, there are no meaningful values to assign to non-responding points. We arbitrarily choose the Y -value of 111 for them. Thus, in total we had 31 data pairs to analyse with our Correlation Ratio algorithm. The Correlation Ratio values ranged from 0 to 1 for the ADM and for the APB mapping.

The computation of Kendall's τ suffered from the same lack of data as the calculation of η – 12 data points were not enough to give stable results. Hence we used the same 19 artificial measurement points as for η and calculated τ for 31 data pairs for each brain point. The values ranged from 0 to 0.72 for the ADM and from 0 to 0.75 for the APB muscle. Figure 3 displays the mapping results for η and τ . As for Experiment 1, we coloured only points within the top 15% range of the mapping values.

The τ map for the APB muscle and the η and τ maps for the ADM muscle show a single, spatially sharply bounded maximum each. The η map for the APB muscle has several maxima, distributed mainly along the central sulcus, but also under the edge of the stimulation area. The coordinates for the maximum mapping values are given in Table II. The distances from the fMRI hot-spots are 6 mm (ADM, η), 5 mm (ADM, τ), 1 mm (APB, η), 3 mm (APB, τ). The distances from the Centre of Gravity maxima are 4 mm (ADM, η), 3 mm (ADM, τ), 5 mm (APB, η), 5 mm (APB, τ). The ADM TMS mapping maxima are located slightly anterior to the fMRI ADM hot-spot, the APB TMS maxima agree with the fMRI APB hot-spot. The distance between the η and τ mapping algorithm is 4 mm for the ADM and for the APB muscle. For the η algorithm the APB-maximum is about 3 mm anterior-lateral to the ADM-maximum. For the τ algorithm the APB-maximum is about 3 mm posterior-lateral to the ADM-maximum. Anatomically, the areas of highest ADM TMS mapping values for η and τ are located on the anterior gyrus close to the central sulcus. The areas of highest APB TMS mapping values are nearly centred at the central sulcus.

Figure 5 shows exemplarily the $(X(\mathbf{p}), Y)$ pairs for three different brain surface points \mathbf{p} and the ADM muscle. The points are chosen such that \mathbf{p}_0 is close to the η and τ maximum, \mathbf{p}_1 is the fMRI hot-spot (having intermediate η and τ value), and \mathbf{p}_2 has low η and τ value.

3.4.3. Experiment 3 The set-up for the third experiment is the standard one for brain mapping: We used a figure-of-eight coil and mapped the MEP responses for a fixed stimulator output. We recorded responses for 46 coil positions and calculated the η , τ , and Centre of Gravity maps. Resulting Correlation Ratio values η ranged from 0 to 0.78. Resulting rank coefficient values τ ranged from 0 to 0.74. The results are displayed in Figure 6. Note that the mapping colours for η and τ to start from 0 and the mapping scale is logarithmic.

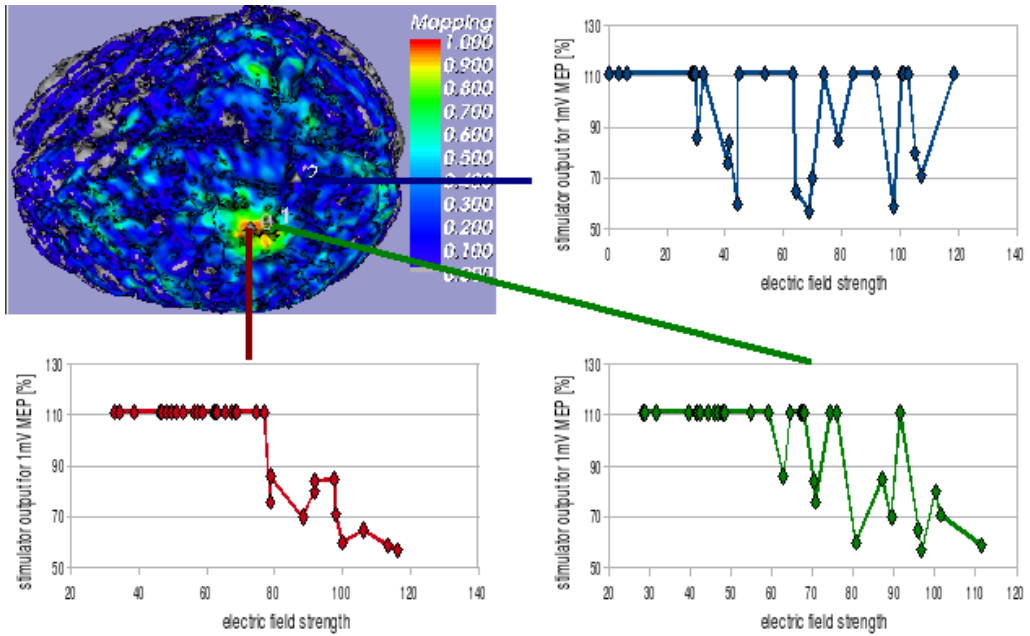


Figure 5. Experiment 2: Calculated electric field strength $X(\mathbf{p})$ (arbitrary units) and respective stimulator output Y (in percent of maximum output) necessary to produce a muscle response of 1mV peak-to-peak at ADM muscle. Y values of 111 indicate that no sufficient stimulation was possible with stimulator output of 100%. The three graphs show the $(X(\mathbf{p}), Y)$ data pairs for three different brain surface points \mathbf{p} , depicted in the upper left picture. The points are chosen such that \mathbf{p}_0 is the Correlation Ration maximum point, \mathbf{p}_1 the fMRI hot-spot, and \mathbf{p}_2 a point with low η and τ value. The Correlation Ratio value at the points is $\eta_0 = 0.98$, $\eta_1 = 0.70$, and $\eta_2 = 0.09$; Kendall's rank coefficient value is $\tau_0 = 0.68$, $\tau_1 = 0.59$, $\tau_2 = 0.26$. The brain in the upper left picture is coloured according to the Correlation Ratio value.

We see that the maps for the η and τ algorithms show a single, spatially sharply bounded maximum each, which agree with each other and are slightly posterior to the Centre of Gravity hot-spot. The maxima are located at the outside of the anterior gyros, ranging into the central sulcus. As Figure 6 shows, there are no “side maxima”, i.e. points outside the central region with high η or τ value.

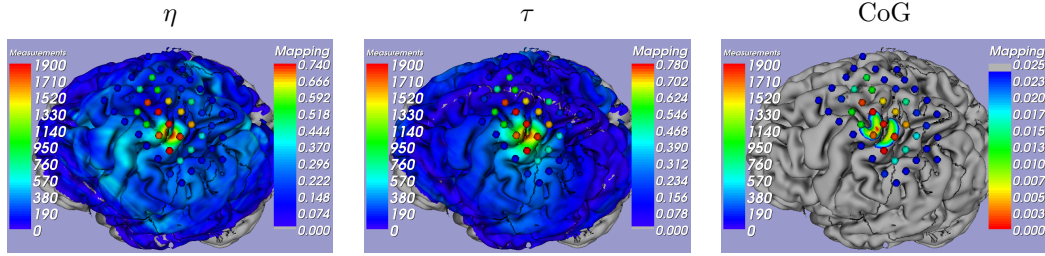


Figure 6. Mapping of the left APB muscle of a second subject with the figure-of-eight coil. Left: Correlation Ratio η values, middle: Kendall's rank coefficient τ values, right: normalised distance from centre of gravity point. The spheres indicate the stimulation positions. The colour of the spheres encodes the obtained MEP signal. For η and τ , the colour of a brain region depicts the mapping value and hence likelihood that the mapped muscle is represented there. Colours range from grey and blue (unlikely) to red (very likely). fMRI data for the subject was not available.

We presented a new approach to brain mapping based on a calculation of a likelihood map using Correlation Ratio η or Kendall's rank coefficient τ . The method allows for the first time mapping with non-focal TMS coils like the Medtronic MCF75 circular coil. The method was tested on two subjects. For the first one, we mapped two hand muscles (ADM and APB) with two coil types (circular coil and figure-of-eight coil) each, using two different mapping approaches. For the second subject, we mapped the APB muscle using a standard figure-of-eight coil.

Core of the η algorithm is a refined Correlation Ratio formula, allowing to get stable results from a very small number of samples (31, 46, and 51 in our case) with continuous range. The algorithm consists of choosing a suitable windowing function for the X -component of the samples and evaluating a rational polynomial expression. The complexity of the algorithm is

$O(n^2)$, n being the number of sample pairs. The main advantage of the new algorithm lies in the capability to yield a good approximation of the theoretical Correlation Ratio value $\eta(Y|X)$ given only very few samples. Because of its direct form, the new Correlation Ratio formula is superior in terms of evaluation speed and stability compared to pure windowing methods, which require numerical integration.

An important feature of the mapping algorithm is the combination of physical responses to stimulation (MEP values) and the electric field produced by the TMS coil. This allows for meaningful mapping resolution of the size of the E-field measurement resolution, see Section 3.2. So even if there are only 30 neurological MEP measurements, spaced with 1 cm distance, the brain mapping resolution is within millimetre range if the coil field is mapped with this accuracy.

The resulting maps give a likelihood that there is a functional (η) or monotonic (τ) dependence between the electric field strength at a point on the cortex and the muscle response to the stimulation. According to our model (Section 3), this translates to a likelihood that the muscle is represented at that point. We remark however, that we use only the maximum point for the prediction of the representation. The question if the extend of high probability values correlates to the area of representation is open and awaits further investigation.

The mapping results are generally in good accordance with alternative mapping methods, see Figures 3 and 6. For Subject 1, the TMS map maxima from Experiment 1 are within 12 mm, the TMS map maxima from Experiment 2 are within 6 mm of the fMRI hot-spots for the representation of the ADM muscle and the APB muscle. The figure-of-eight mappings for both Subjects (Experiments 2 and 3) also agree closely with the established Centre of Gravity mapping, [6]. All maps have their maximum close to an area which is known as the hand knob

in anatomy [31]. Hence the general localisation from our algorithm is correct. When comparing ADM and APB localisation in Subject 1, we find that the ADM muscle is represented slightly more medial as the APB muscle, complying with the results from literature [32].

The comparison of Correlation Ratio mapping (η) and rank coefficient mapping (τ) revealed little difference in localisation. The maxima of both methods were only 4 to 6 mm apart, with the high probability areas for the representation mainly overlapping (coloured areas in Figure 3). Overall, the maps produced by taking Kendall's τ as a measure were a bit smoother and did not suffer from any side maxima like the η APB mapping in Experiment 2.

As the results in Section 3.4 show, the mapping is generally of good quality, but it is not perfect:

1. TMS mapping values of the fMRI hot-spots for the circular coil experiment are not the maximum values.
2. The region of high mapping values for the circular coil maps extend posterior into the postcentral gyrus.
3. Separate small spots of high Correlation Ratio value appear also far away from the correct localisation. This is most pronounced for the map of the APB muscle in Subject 1 with the figure-of-eight coil.

The following paragraphs discuss possible explanations for the three mapping problems.

For the first problem, our initial assumption, that the MEP amplitude Y is a monotonic function of the electric field strength X at the representation point \mathbf{p}^r , is not strictly valid. Several reports exist, that also the direction of the field influences the strength of the muscle response [33, 34]. This explanation is also supported by Figure 4, showing no clear monotonic

functional dependence between $X(\mathbf{p})$ and Y , even for a point close to the ADM representation. Note that mapping with the circular coil implies the electric field vector at the representation point \mathbf{p}^r changes orientation by full 360° when placing the coil along a circle around \mathbf{p}^r . Fox et. al. suggested a direct dependence of the MEP amplitude on the field strength and the angle between the electric field and the brain surface normal at the representation point [20], a finding unconfirmed by other researchers.

We remark here that the number of three stimuli averaged at every stimulation point is rather low. This might also impair the quality of the maps, as the calculated mean MEPs are only rough estimates of the “real” MEPs. This could at least partially explain the deviation from a monotonic relationship between electric field strength at the representation point and the MEP responses as seen in Figure 4. Further, the restriction to precentral stimulation sites in Experiment 1 might also have impaired the mapping. Incorporating postcentral stimulation points should enhance it, because it increases the diversity of the $(X(\mathbf{p}), Y)$ data pairs. For the figure-of-eight coil, additional measurements may make the use of artificial stimulation results obsolete.

Finally, our algorithm does not account for electric field distortions produced by the head. Further research will incorporate field simulations to approximate the true electric field distribution in the head better and allow comparison of the original mapping algorithm presented here and a distortion corrected one. As explained in Section 3.3 we do not expect big differences, but we are not yet able to quantify this.

Regarding problem two, the extension of the Correlation Ratio maps to the postcentral gyrus in the case of mapping with the circular coil, we believe that this is mainly due to the restriction to precentral stimulation regions. We hope that after changing the laboratory setup

to map patients in a comfortably sitting position we will be able to stimulate points all around the head and thus produce more focal mappings. But it is also possible that we need to incorporate some E-field directional dependence in our formula, as discussed above.

We remark that the distance between the precentral and the postcentral gyrus is only about 5mm – 10mm, as the patient's MRI revealed. Hence our TMS maps seem accurate to about this degree. This performance is especially remarkable given that the stimulation data was not optimal. The circular coil experiments lacked postcentral stimulation points and the experiments with the figure-of-eight coil had only a very limited number of 12 stimulation points. Furthermore, we boldly approximated the electric field in the brain by the electric field in air, as explained in Section 3.3. The fact that we got correct mapping results, despite the approximations and the sub-optimal data, shows the robustness of both, the new Correlation Ratio formula from Section 2.2 and the overall mapping method.

Problem three seems to be related to the broad nature of the Correlation Ratio as a measure. Any functional dependence between X and Y leads to $\eta(Y|X) = 1$. Hence there might be points \mathbf{p} on the brain surface exhibiting by chance a functional relationship between electric field strength $X(\mathbf{p})$ and MEP values Y . Our experience, however, is that the number and the CR-value of these “false positive” spots decreases with more measurements. This is the reason we included the 15 and 12 artificial measurements, in Experiment 1 and 2, respectively, into the data pairs.

As a test of this “more measurements decrease the number of ‘false positives’” – hypothesis, we mapped the APB of Subject 2 using 46 stimulation points with the MagStim figure-of-eight coil (Experiment 3, Section 3.4.3). The resulting Correlation Ratio values are displayed in Figure 6. We see that there is now only one maximum area, namely at the outer side of the

hand knob.

The presented experimental data can only be seen as a pilot study regarding applicability and accuracy of the proposed mapping method. Further data of more subjects are necessary to confirm our findings. Furthermore, we like to extend the experiments to highly un-focal coils like the H-coil to demonstrate that our algorithms can handle any coil type as long as its electric field characteristics are known.

Future work will also incorporate comparison with direct electrical stimulation during neurosurgery, as Krings et. al. suggested [35]. Furthermore, we work on optimising the E-field measurements for the TMS-coils. The oscilloscope used in Section 3.2 has only a data range of 1 Byte, although adjustable in the measurement range, limiting the resolution of the electric field measurements. Additionally, we work on simulating electric fields of the coils, as described in [36], to quantify effects of field distortion in the head.

REFERENCES

1. Barker AT, R J, Freeston IL. Non-invasive magnetic stimulation of human motor cortex. *Lancet*. 1985 May;8437(1):1106–7.
2. Brasil-Neto JP, Cohen LG, Panizza M, Nilsson J, Roth BJ, Hallett M. Optimal focal transcranial magnetic activation of the human motor cortex: effects of coil orientation, shape of the induced current pulse, and stimulus intensity. *J Clin Neurophysiol*. 1992 Jan;9(1):132–136.
3. Ettinger GJ, Leventon ME, Grimson WEL, Kikinis R, Gugino L, Cote W, et al. Experimentation with a transcranial magnetic stimulation system for functional brain mapping. *Medical Image Analysis*. 1998;2(2):133–42.
4. Herwig U, Kölbel K, Wunderlich AP, Thielscher A, v Tiesenhausen C, Spitzer M, et al. Spatial congruence of neuronavigated transcranial magnetic stimulation and functional neuroimaging. *Clinical Neurophysiology*. 2002;113:462–8.
5. Okamoto M, Dan I. Automated cortical projection of head-surface locations for transcranial functional

- brain mapping. *Neuroimage*. 2005 May;26(1):18–28. Available from: <http://dx.doi.org/10.1016/j.neuroimage.2005.01.018>.
6. Classen J, Knorr U, Werhahn KJ, Schlaug G, Kunesh E, Cohen LG, et al. Multimodal output mapping of human central motor representation on different spatial scales. *J Physiol*. 1998 Oct;512 (Pt 1):163–179.
 7. Pascual-Leone A, Davey NJ, Rothwell J, Wassermann EM, Puri BK. *Handbook of Transcranial Magnetic Stimulation*. Arnold; 2002.
 8. Roth Y, Zangen A, Hallett M. A Coil Design for Transcranial Magnetic Stimulation of Deep Brain Regions. *Journal of Clinical Neurophysiology*. 2002;19(4):361–70.
 9. Thielscher A, Kammer T. Linking Physics with Physiology in TMS: A Sphere Field Model to Determine the Cortical Stimulation Site in TMS. *NeuroImage*. 2002;17(3):1117–30.
 10. Nadaraya EA. On estimating regression. *Theory Prob Applic*. 1964;10:186–90.
 11. Watson GS. Smooth regression analysis. *Sankhya*. 1964;A 26:101–6.
 12. Pearson K. On the General Theory of Skew Correlation and Non-linear Regression. *Drapers' Company Research Memoirs*: Dulau and Co. 1905;.
 13. Roche A, Malandain G, Ayache N. The Correlation Ratio as a New Similarity Measure for Multimodal Image Registration. In: Proc. of First Int. Conf. on Medical Image Computing and Computer-Assisted Intervention (MICCAI'98). vol. 1496 of Lecture Notes in Computer Science. Cambridge, USA: Springer Verlag; 1998. p. 1115–24.
 14. Papoulis A, Pillai SU. *Probability, Random Variables and Stochastic Processes*. 4th ed. McGraw-Hill, Inc.; 2002.
 15. Press WH, Teukolsky SA, Vetterling WT, Flannery BP. *Numerical Recipes in C++: The Art of Scientific Computing*. 2nd ed. Cambridge, UK: Cambridge University Press; 2002.
 16. Kelley TL. An Unbiased Correlation Ratio Measure. *Proceedings of the National Academy of Sciences of the United States of America*. 1935;21(9):554–9.
 17. Fox J. *Nonparametric Simple Regression: Smoothing Scatterplots*. Sage Publications; 2000.
 18. Takezawa K. *Introduction to Nonparametric Regression*. Wiley-Interscience; 2006.
 19. Parzen E. On Estimation of a Probability Density Function and Mode. *The Annals of Mathematical Statistics*. 1962;33(3):1065–76.
 20. Fox PT, Narayana S, Tandon N, Sandoval H, Fox SP, Kochunov P, et al. Column-based model of electric field excitation of cerebral cortex. *Hum Brain Mapp*. 2004 May;22(1):1–14.
 21. Matthäus L, Giese A, Wertheimer D, Schweikard A. Planning and Analyzing Robotized TMS Using

- Virtual Reality. In: Medicine Meets Virtual Reality 14: Accelerating Change in Healthcare: Next Medical Toolkit. vol. 119 of Stud Health Technol Inform. IOS Press; 2005. p. 373–8.
22. Matthäus L, Fadini T, Trillenberg P, Giese A, Rasche D, Bodensteiner C, et al. Robotised Transcranial Magnetic Stimulation. *IEEE Transactions on Robotics*; Submitted.
 23. Nayfeh MH, Brussel MK. Electricity and Magnetism. New York: Wiley; 1985.
 24. Malmivuo J, Plonsey R. Bioelectromagnetism: Principles and Applications of Bioelectric and Biomagnetic Fields. New York: Oxford University Press; 1995.
 25. Epstein CM, Schwartzberg DG, Davey KR, Sudderth DB. Localizing the site of magnetic brain stimulation in humans. *Neurology*. 1990 Apr;40(4):666–70.
 26. Rudiak D, Marg E. Finding the depth of magnetic brain stimulation: a re-evaluation. *Electroencephalogr Clin Neurophysiol*. 1994 Oct;93(5):358–371.
 27. Salinas FS, Lancaster JL, Fox PT. Detailed 3D models of the induced electric field of transcranial magnetic stimulation coils. *Phys Med Biol*. 2007 May;52(10):2879–2892.
 28. Nunez P, Srinivasan R. Electric Fields of the Brain: The Neurophysics of EEG. 2nd ed. Oxford University Press; 2006.
 29. Friston KJ, Holmes AP, Poline JB, Grasby PJ, Williams SC, Frackowiak RS, et al. Analysis of fMRI time-series revisited. *Neuroimage*. 1995 Mar;2(1):45–53. Available from: <http://dx.doi.org/10.1006/nimg.1995.1007>.
 30. Rorden C. MRIcro software;. Version 1.40. www.mricro.com.
 31. Yousry TA, Schmid UD, Alkadhi H, Schmidt D, Peraud A, Buettner A, et al. Localization of the motor hand area to a knob on the precentral gyrus. A new landmark. *Brain*. 1997 Jan;120 (Pt 1):141–157.
 32. Bähr M, Frotscher M. Duus' Neurologisch-topische Diagnostik. 8th ed. Georg Thieme Verlag; 2003.
 33. Kammer T, Beck S, Thielscher A, Laubis-Herrmann U, Topka H. Motor thresholds in humans: a transcranial magnetic stimulation study comparing different pulse waveforms, current directions and stimulator types. *Clin Neurophysiol*. 2001 Feb;112(2):250–58.
 34. Brasil-Neto JP, McShane LM, Fuhr P, Hallett M, Cohen LG. Topographic mapping of the human motor cortex with magnetic stimulation: factors affecting accuracy and reproducibility. *Electroencephalogr Clin Neurophysiol*. 1992 February;85(1):9–16.
 35. Krings T, Buchbinder BR, Butler WE, Chiappa KH, Jiang HJ, Rosen BR, et al. Stereotactic transcranial magnetic stimulation: correlation with direct electrical cortical stimulation. *Neurosurgery*. 1997 Dec;41(6):1319–25; discussion 1325–6.

36. Roth BJ, Saypol JM, Hallett M, Cohen LG. A theoretical calculation of the electric field induced in the cortex during magnetic stimulation. *Electroencephalogr Clin Neurophysiol*. 1991 Feb;81(1):47–56.